Surface ligand assisted valence change in ceria nanocrystals

J. Zhang,[1] T. Naka,[1,2,*] S. Ohara,[1,3] K. Kaneko,[4,5] T. Trevethan,[6,7] A. Shluger,[6,7] and T. Adschiri[6]

[1]*Institute of Multidisciplinary Research for Advanced Materials, Tohoku University, Sendai 980-8577, Japan*

[2]*National Institute for Materials Science, Tsukuba, Ibaraki 305-0047, Japan*

[3]*Joining and Welding Research Institute, Osaka University, Ibaraki, Osaka 567-0047, Japan*

[4]*Department of Materials Science & Engineering, Kyushu University, Fukuoka 819-0395, Japan*

[5]*Core Research for Evolutional Science and Technology, Kyushu University, Fukuoka 819-0395, Japan*

[6]*WPI-Advanced Institute for Materials Research, Tohoku University, Sendai 980-8577, Japan*

[7]*Department of Physics and Astronomy, University College London, Gower Street, London WC1E 6BT, United Kingdom*

(Received 10 March 2011; published 6 July 2011)

In this report, we used x-ray absorption, electron energy-loss, and magnetic analyses to demonstrate the effect of modification of ceria ($CeO_{2-\delta}$) nanocrystals with a particle size $D = 3.5$–14 nm by oleic acid surface ligands. We observe a shift of the electronic state of the cerium ions from tetra to trivalent state as the surface density of the ligand molecules is increased. The valence state of cerium in the nanocrystal is strongly correlated with the number of ligand molecules bound to the surface of the ceria nanocrystals. One oxygen vacancy is stabilized by 5–6 ligand molecules bound on a $CeO_{2-\delta}$ nanocrystal.

DOI: 10.1103/PhysRevB.84.045411 PACS number(s): 61.46.Df, 81.07.Bc, 73.22.Dj, 71.30.+h

I. INTRODUCTION

Many of the physical and chemical properties of metal oxides, which are critical to a wide range of technological applications, can be controlled by inducing changes in the oxygen content of these compounds. For example, metal oxides with off-stoichiometric oxygen content have exhibited high-T_c superconductivity,[1] metal-insulator transitions,[2] and colossal magnetoresistance.[3] Moreover, changes in the oxygen content in such materials can promote and enhance catalytic activity[4,5] and ionic conduction.[6] Both static and dynamic changes in the valence of metal ions that occur at the interface between a metal oxide material and its environment can significantly influence its oxygen storage and transport capabilities, and this is particularly relevant in the case of nano-structured materials and nanoparticles with large surface areas. In this regard, cerium oxide (ceria) nanoparticles have received much attention owing to their remarkable ability to store and transport oxygen. The processes that underpin this ability are associated with a fast valence change in the compound, i.e., $Ce^{4+} \leftrightarrow Ce^{3+}$, and are often attributed to the creation of anionic vacancies, i.e., $CeO_2 \rightarrow CeO_{2-x} + (x/2)O_2$.

The synthesis of such metal oxide nanocrystals—with control over their size, shape, and surface features—is of fundamental technological interest because it is possible to tune both the size- and shape-dependent physical properties and also to prevent nanoparticle aggregation in a solvent. Recently, the organic-solution phase[7–9] and liquid–solid–solution phase synthetic-transfer routes[10] have been demonstrated to provide versatile pathways toward the controlled synthesis of metal oxide nanocrystals. In these methods organic surfactants can play a key role in controlling both the growth and stability of nanocrystals. Combining this concept and the properties of sub- and supercritical water (SCW) has lead to a novel approach for the synthesis of metal oxide nanocrystals. For example, SCW is chemically stable and processing with it is environmentally benign;[11] it acts as a unique medium to aid in the spontaneous nucleation and crystallization of metal oxide nanoparticles;[12] and by using organic ligand molecules that are miscible with SCW, crystal growth can be limited and agglomeration can be inhibited in favor of small, well-dispersed particles.[13,14] Additionally, since at the vicinity of the super critical point (374 °C, 22.1 MPa) where the properties of water change drastically, reaction equilibrium, adsorption equilibrium, and solubility also change remarkably; unique crystalline and surface bonding characteristics can be obtained. Under hydrothermal conditions in the presence of an organic surface modifier, a metallic source oxidizes and forms oxide nanocrystals since crystal growth (Ostwald ripening) is suppressed owing to the low solubility of oxides in super- or subcritical water. During crystallization the surface of the growing metal oxide interacts with and is modified by the organic-surface modifiers. This so-called *in-situ* surface modification is advantageous because it changes the surface nature of the nanocrystals from hydrophilic to hydrophobic and vice versa.[15,17]

In this paper we report that the tetra-to-trivalent transformation in ceria nanoparticles is facilitated by organic ligand molecule bonding on the exposed surfaces of the crystals and that this can occur at nanoparticle diameters significantly above $D = 3$ nm. It is well known that when the diameter of ceria nanoparticles decreases below approximately 3 nm, the average lattice constant of the crystal structure (a) begins to increase. Studies by Tsunekawa *et al.*,[18,19] Wu *et al.*,[20] Deshpande *et al.*,[21] and F. Zhang *et al.*[22] have indicated that trivalent cerium ions (Ce^{3+}) become dominant in the nanoparticles when the particle size decreases below this critical diameter, and that this change in valence is linked to the increase in lattice constant. However, large discrepancies in the precise relationship between the lattice constant and particle diameter between these different studies suggest that the cerium valence is not just a simple function of D. In fact, the cerium valence transformation may also depend on the nature of particle surfaces; i.e., the morphology of nanocrystals[18,19] and the termination of the crystal structure at exposed surfaces.[23]

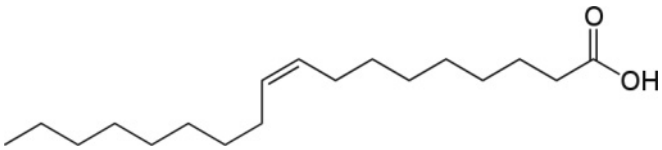

FIG. 1. Molecular structure of the oleic acid surface modifier.

Here we employed *in-situ* surface modification to synthesize ceria nanocrystals modified by oleic acid, which is a nontoxic fatty (hydrophobic) acid found in various vegetable and animal sources with a chain length of 2.2 nm (see Fig. 1). Quantitative analysis employing x-ray diffraction (XRD), electron energy-loss spectroscopy (EELS), Fourier transform infrared (FT-IR) spectra, and thermogravimetric–differential thermal analysis (TG-DTA) reveal that both the proportion of trivalent cerium (and the corresponding oxygen-vacancy concentration) and the lattice spacing are strongly correlated with the number of the ligand molecules adsorbed on the surfaces of the nanoparticles.

This approach to ceria nanoparticle synthesis demonstrates how both the oxygen content and the morphology of the ceria nanoparticles, both of which are critical to their reactivity and oxygen storage capacity, can be controlled through a careful choice of organic surface modifier. The plan of the remainder of the paper is as follows: in the next section we describe the methodology for sample preparation. Then in the following section we describe in detail the results of each of the analytical methods we employ (the details of which are included in as supplementary information). Finally we present a discussion of the results and conclusions.

II. EXPERIMENTAL METHODS

In a typical nanoparticle synthesis, the cerium oxide precursor was prepared by mixing 100 ml of 0.1 M $Ce(NO_3)_3$ solution with 100 ml of 0.3 M NaOH. After the reaction mixture had been stirred for approximately 6 h, the precursor was centrifuged and washed several times with distilled water. To synthesize nonmodified ceria nanocrystals, the 0.02-M precursor was transferred into a pressure-resistant SUS316 vessel (inner volume, 5 ml). The hydrothermal reaction was performed in the reactor for 10 min at a temperature range of 200–500 °C. A series of nonmodified nanocrystals with sizes of ∼2 to ∼15 nm was obtained by increasing the temperature of the reaction. To compare the influence of the surface ligands on the structural behavior of the ceria nanocrystals, an amount of oleic acid (in the range of 0.05–1 g) was also loaded into the vessel reactor. The hydrothermal reaction was then performed in the reactor at 400 °C for 10 min, as reported previously.[15] The nanocrystal size was managed by controlling the concentration of organic ligands in the reaction mixture.

XRD patterns were recorded on a RINT-2000 spectrometer (Rigaku, Tokyo, Japan) with Cu-Kα radiation. The samples were ground to fine powders before being subjected to XRD measurement. Transmission electron microscopy (TEM) images were obtained with a transmission electron microscope (JEM-1200EX, Japan) operated at 120 kV. High-resolution TEM (HRTEM) characterization was carried out using a Hitachi H-7100 electron microscope operating at 200 kV. The samples used for TEM and HRTEM measurements were dispersed in tetrahydrofuran (∼0.1 weight%) before being transferred to carbon-coated copper grids. Thermogravimetric–differential thermal analysis (TG–DTA) was performed with a Thermo Plus TG8120 Rigaku instrument that was heated from room temperature to 100 °C at a rate of 10 °C min^{-1}. After maintaining a temperature of 100 °C for 30 min, the temperature was increased to 300 °C at a rate of 10 °C min^{-1} and maintained for 30 min again before heating to 800 °C at a rate of 10 °C min^{-1}. CaO was used as a reference compound for TG–DTA. FT-IR spectra were obtained on an FT-IR spectrometer (680 plus; FTIR JASCO Co.) at a resolution of 4 cm^{-1}. X-ray absorption near-edge structure (XANES) spectra at the Ce L_3-edge were carried out at ambient conditions in BL-7C (Photon Factory, KEK). To suppress unwanted harmonics, the angle between the monochromatic crystal faces was adjusted to mistune the incident beam by 30%. The incident and output-beam intensities were monitored and recorded using 30% helium-doped nitrogen gas and a nitrogen-flowing ionization chamber. The spectra were scanned in the range of 5.5–6.2 keV, which covers the L_3-edge absorption of cerium atoms. The samples were examined by field-emission TEM at 300 kV (TECNAI-30F with a postcolumn energy filter and a JEM-3200FSK with an in-column energy filter). The oxidation states were examined by EELS with energy resolution better than 0.9 eV. To measure the EELS edges, the beam width was maintained at approximately a few nanometers. Since electron beam irradiation might result in the loss of oxygen in ceria nonocrystals,[20] we determined an appropriate shorter irradiation time during EELS measurement. Magnetic measurements were carried out on a superconducting quantum interference device (SQUID) magnetometer (Quantum Design, MPMS) under a magnetic field up to 50 kOe in the temperature range between 4 and 100 K.

III. EXPERIMENTAL ANALYSIS

A. Crystallographic and morphological evolutions

Figure 2(a) shows XRD profiles for the synthesized products along with the simulated profiles for CeO_2 (with the fluorite structure) and the C-type $Ce_2O_{3-\delta}$.[24] All of the reflection peaks can be assigned to the cubic fluorite structure of ceria with respective lattice parameters. In the case of the unmodified nanocrystals, the crystal diameter was estimated from the line width by using Scherrer's equation and increases with increasing reaction temperature. As shown in Fig. 2(b), the lattice constant a is independent of nanoparticle diameter above 3.5 nm and corresponds to that of bulk stocheometric CeO_2 (a = 5.41 Å). However, in case of the modified nanocrystals, the lattice constant increases for nanocrystal sizes up to 7 nm, although the increment of a as a function of D for the modified nanocrystals is considerably smaller than those previously reported[18–21] but comparable with that obtained by Zhang *et al.*[22]

As stated previously, earlier studies[18–22] have indicated that the proportion of trivalent cerium significantly increases when the particle size decreases below a few nanometers. However, as shown in Fig. 2(b), here we observed significant differences in the relationship between the lattice constant

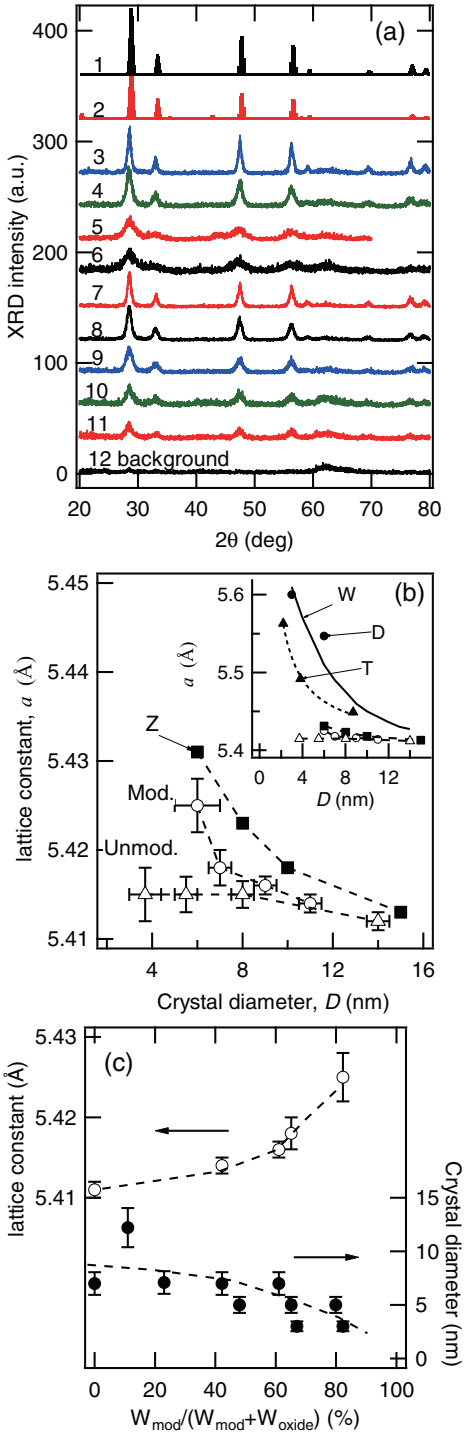

FIG. 2. (Color online) (a) XRD profiles 1 and 2 are simulated for CeO_2 (fluorite) and C-Ce_2O_3, respectively. The profiles 3–6 are of $CeO_{2-\delta}$ nanocrystals synthesized at 500, 400, 260, and 200 °C without the modifier, respectively. The profiles 7–11 are of $CeO_{2-\delta}$ nanocrystals synthesized with the molar ratio of the modifier to the metal precursor 4.5, 10.5, 18.9, 31.5, and 94.5, respectively. (b) Lattice constants as a function of particle size for ceria nanocrystals prepared by several research groups (denoted by T,[18,19] W,[20] D,[21] and Z[22]) and in the present study both with (Mod.) and without (Unmod.) organic modifiers. (c) Weight ratio of the modifier $R_{sm} = W_{mod}/(W_{mod} + W_{oxide})$ dependence on lattice constant and crystal size D.

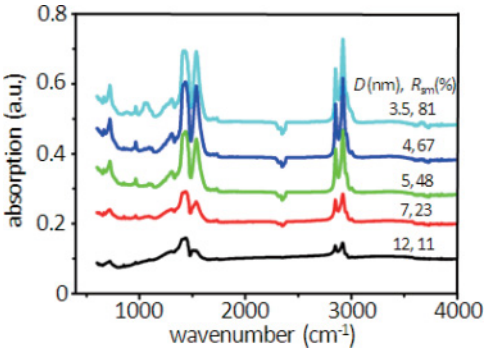

FIG. 3. (Color online) FT-IR spectra of the surface modified nanocrystals at various crystal diameters D and weight ratios R_{sm} for the surface modified ceria nanocrystals.

and D when we compared our present results with the results of these previously published studies. This suggests that the lattice expansion $\Delta a/a$, because of the valence transformation, depends not only on D but also on other quantities. As discussed in subsequent detail, we found that the cerium valence transformation (from Ce^{4+} to Ce^{3+}) depends strongly on both the particle's morphology and the surface modification by the oleic acid ligands.

B. FT-IR spectroscopy and Thermogravimetric–differential thermal analysis

The FT-IR spectra of ceria nanocrystals with varying degrees of oleic acid surface ligand coverage indicate that the chemical bonding between the surface ligands and the ceria surface is changed with increasing molecular coverage R_{sm} (Fig. 3). Here the coverage is defined according to the weight ratio of the modifier $R_{sm} = W_{mod}/(W_{mod} + W_{oxide})$ employed in the synthesis. Interestingly, Fig. 3 implies that the morphology of the ceria nanocrystals is transformed with increasing R_{sm} on the basis of the calculated binding structures described shortly. Spectral bands in the 2800–2960 cm^{-1} region are attributed to the C–H stretching mode of methyl and methylene groups (Fig. 3). It is worth noting that bands at 1532 and 1445 cm^{-1}, which are characteristic of the asymmetric (COO^-) and symmetric (COO^-) stretching modes, respectively, are present in the spectra of the ceria nanocrystals with surface ligands. The presence of these bands indicates that oleic acid is bound to the ceria nanocrystals as a form of carboxylate,[25–28] which can stabilize the Ce^{3+} state. With the decreasing of the nanocrystal size [Fig. 4(f)] and the change in morphology from cubic to truncated-cubic, as shown in Fig. 4(b)–4(e), the intensity ratio of (COO^-) at 1532 cm^{-1} to (COO^-) at 1445 cm^{-1} was enhanced, implying that the binding properties of the surface ligands on the ceria nanocrystals have changed.

The TG–DTA curves showed two distinct transitions between the room temperature and 800 °C for all samples tested [see typical results in Fig. 5(a)]. The first weight-loss peak, which occured around 290 °C, reveals that the oleate ligands dissociated from the surface of the ceria nanocrystals. The weight-loss peak at around 400 °C, corresponding to a chemical bonding between the organic ligands and the surface

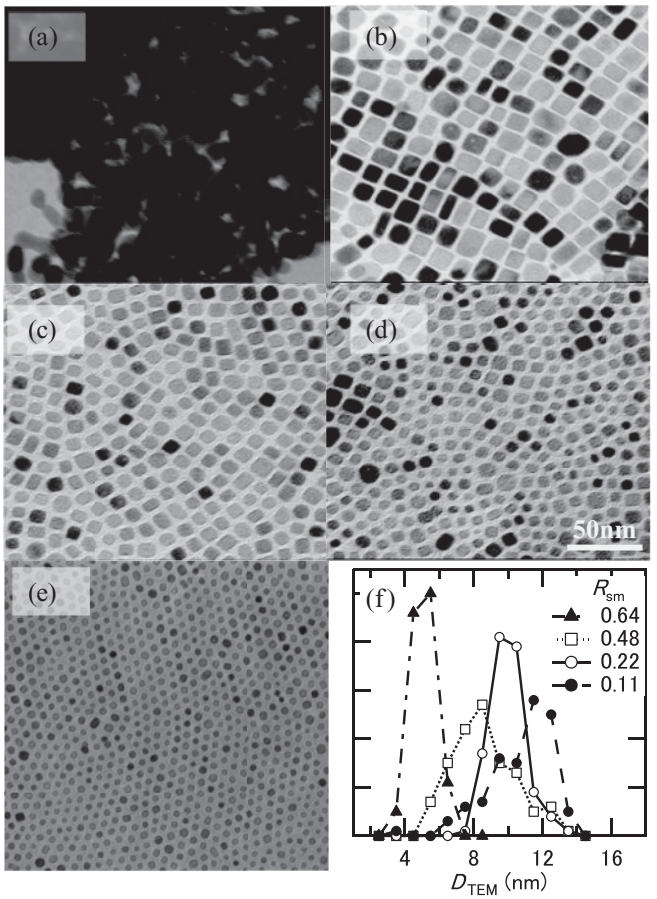

FIG. 4. TEM images of surface-modified ceria nanoparticles with surface ligand densities of $R_{sm} = 0$ (a), 0.11 (b), 0.22 (c), 0.48 (d), and 0.64 (e), respectively. Scale bar is 50 nm for all four panels. (f) Crystal size dispersion profiles for the respective R_{sm}. Lines between data points are the guides for eyes.

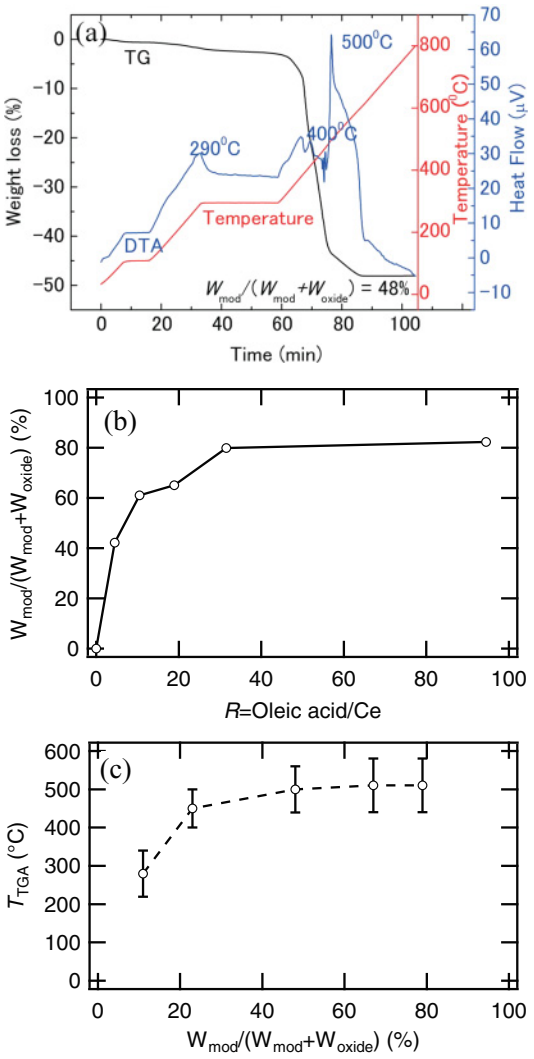

FIG. 5. (Color online) (a) TG–DTA curves (weight loss) for ceria nanocrystals with $R_{sm} = 48\%$. The curves were obtained at a heating rate of 10 °C/min. (b) Weight ratio of bonding organic molecule on ceria nanocrystals as a function of a molar ratio of surface ligand molecule and cerium ion in the precursor. (c) Dissociation point of the bonding organic molecules, T_{TGA}, as a function of weight ratio of the bonding organic molecules.

of the ceria nanocrystals,[29,30] was enhanced markedly with decreasing the ceria nanocrystal size. Remarkably these results indicate that the coverage of the ligands is increased with decreasing particle size, as shown in further discussion. This suggests that the morphology of the ceria nanocrystals depends strongly on the nature of the bonding interaction between the ceria surface and the organic ligands. Furthermore the binding state at the interface and the observed adsorption energy explain well the changing intensity ratio of the two peaks observed in the FT-IR spectra.[16]

C. Valence changes

The valence state of the ceria nanocrystals was evaluated by Ce L_3-edge XANES analysis, transmission electron microscopy with electron energy-loss spectroscopy (TEM-EELS), and magnetic susceptibility SQUID measurements under ambient conditions. XANES and TEM-EELS allow for direct observation of the cerium valence state. Figure 6(a) and (b) show Ce L_3-edge XANES spectra of the ceria nanoparticles. For comparison we also obtained Ce L_3-edge XANES spectra of the reference compound cerium(III) stearate ($Ce(C_{18}COO)_3$) and of bulk stoichiometric cerium(IV) oxide (CeO_2). The strongest peak (C) [assigned in Fig. 6(b)] observed for cerium(III) stearate is attributed to the dipole-allowed transition of Ce 2p to Ce $4f^1 5d$,[31–34] and this peak was assumed to correspond to trivalent cerium in the ceria nanocrystals. The cerium(IV) oxide XANES spectrum has a distinct double-peak structure (D,E) [assigned in Fig. 6(a)], and these peaks are attributed to the Ce 2p to 5d $L4f^1$ and 2p to $4f^0$ configurations, respectively, where L indicates a ligand (oxygen) hole. Using fitting procedures,[35,36] we obtained average valence transitions from the spectra of ceria nanocrystals of various sizes. As shown in Fig. 6(a), no significant change in the valence of cerium was observed for nonmodified ceria nanocrystals with particle sizes above 3 nm. In contrast when the surfaces of the nanocrystals were modified by organic ligands, their spectroscopic valence varied from +3.54 to +3.10 with decreasing particle size [Fig. 6(d)].

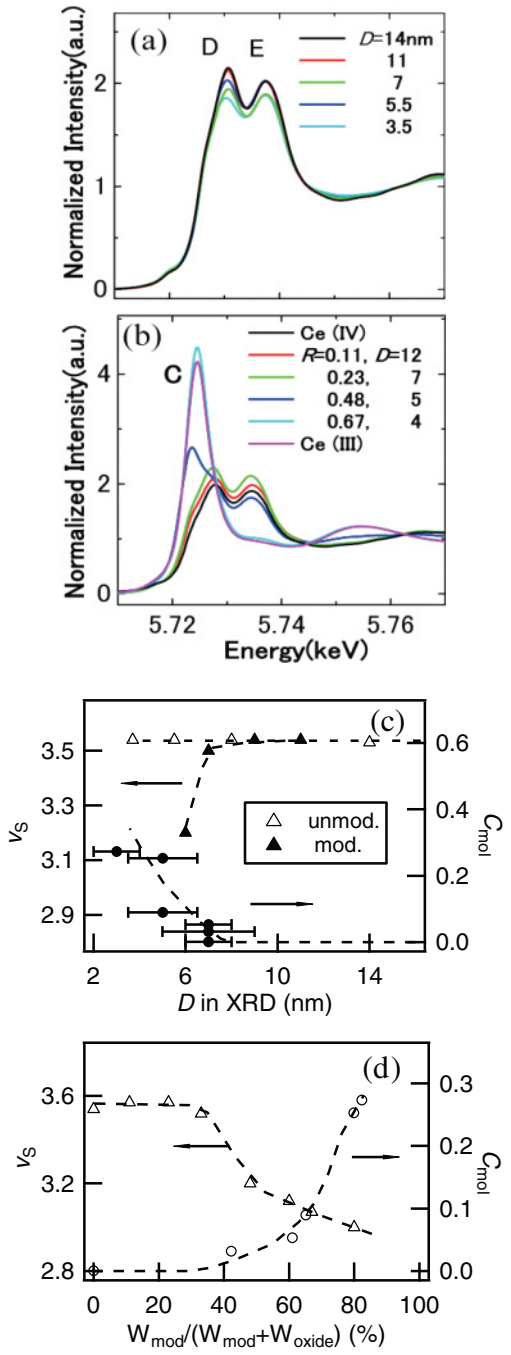

FIG. 6. (Color online) Ce L_3-edge XANES of ceria nanocrystals (a) without and (b) with surface ligands. Those of the reference compound cerium(III) stearate ($Ce(C_{18}COO)_3$) and of bulk cerium(IV) oxide (CeO_2) are also shown for comparison. The spectroscopic valence of cerium ions and Curie constant in the unit of emu/K mol estimated below 30 K (c) as a function of particle size and (d) as a function of weight ratio of the ligand molecule. Dashed lines are used to guide the eye.

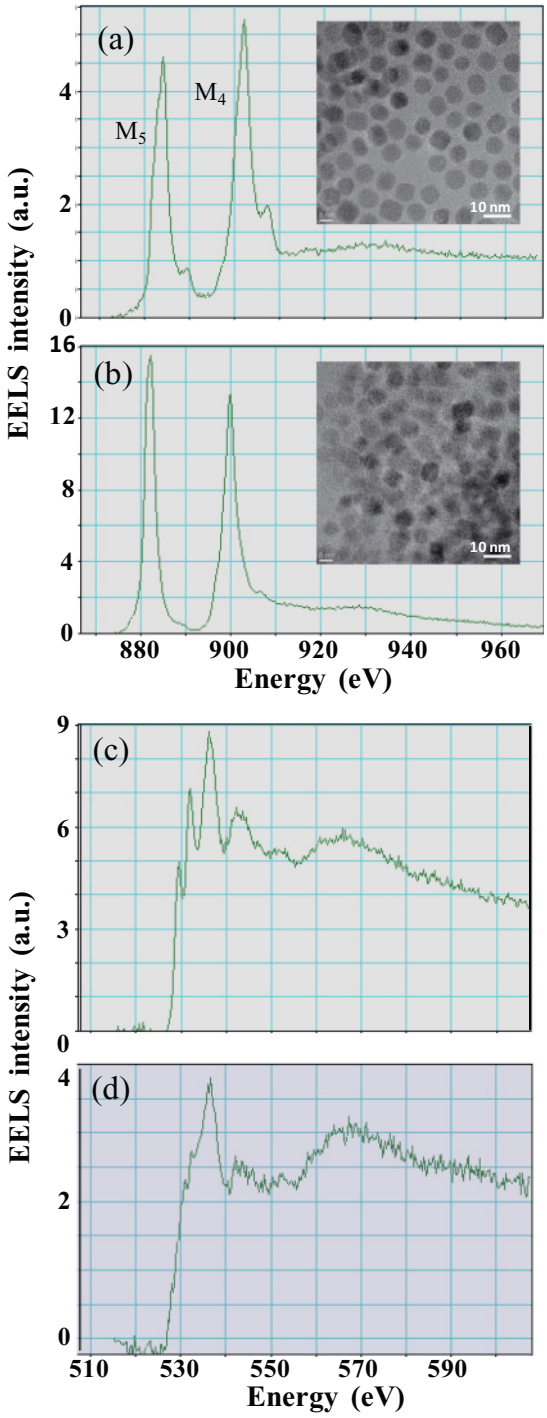

FIG. 7. (Color online) (a–d) TEM-EELS spectra of Ce $M_{4,5}$-edge with $R_{sm} = 0.33$ (a) and $R_{sm} = 0.67$ (b) and of O K-edges with $R_{sm} = 0.33$ (c) and $R_{sm} = 0.67$ (d). The TEM images from which these EELS spectra were obtained are shown in the insets of (a) and (b) for $R_{sm} = 0.33$ and 0.67, respectively.

To examine the valence state of the samples at the nanoscale, we also acquired TEM-EELS spectra [Fig. 7(a)–7(d)]. The TEM images from which the spectra were acquired are shown in the insets of Fig. 7(a) and 7(b). Within the Ce $M_{4,5}$-edge, two major peaks were observed for ceria nanocrystals with a surface ligand density of $R_{sm} = 0.33$ and 0.67, as shown in Fig. 7(a) and 7(b), respectively. The shape and position of these two peaks, referred to as M_5 and M_4, differed between the two ceria nanocrystal samples. For the sample with $R_{sm} = 0.67$, the positions of the peaks were shifted to a lower-energy region relative to those observed for the sample with $R_{sm} = 0.33$. Furthermore the M_5 and M_4 energy maxima were greater at $R_{sm} = 0.67$ than at $R_{sm} = 0.33$, and the intensity

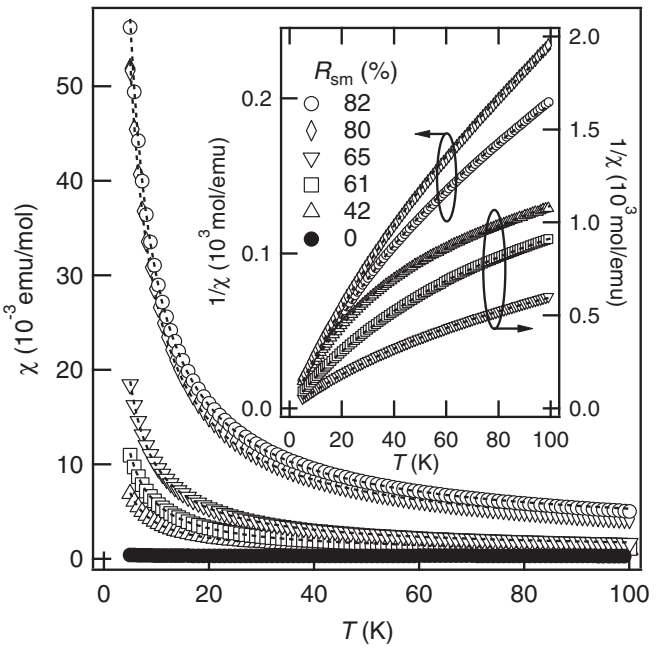

FIG. 8. (a) Temperature dependence of magnetic susceptibility of ceria nanocrystals with various weight ratios R_{sm}. Inset shows the reciprocal susceptibility at various weight ratios as a function of temperature. Dashed lines represent the fitted lines based on the crystal field scheme for the 4f-moment ($J = 5/2$) on Ce^{3+} in the cubic crystal ligand field with Γ_7 doublet (ground state) and Γ_8 quartet (excited state). The latter locates at Δ in energy above the ground state.

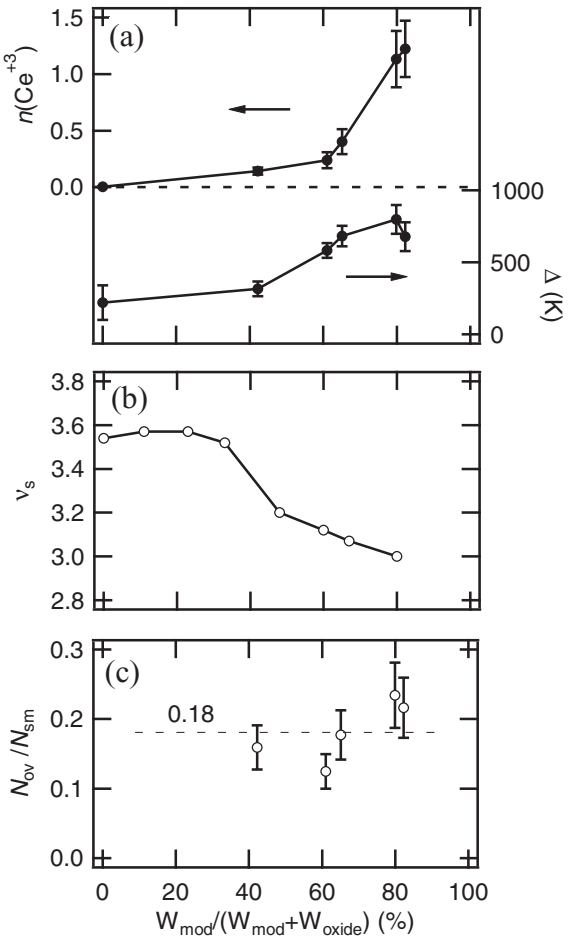

FIG. 9. The weight ratio's R_{sm} dependence of (a) the concentration of Ce^{3+}, $n(Ce^{3+})$ and the crystal field splitting Δ, (b) spectroscopic valence of cerium ion, and (c) ratio of number of oxygen vacancy N_{ov} to number of surface bonding molecule per crystal N_{sm}.

ratio for the two peaks was inverted such that M_5 was more intense for the $R_{sm} = 0.67$ sample relative to the $R_{sm} = 0.33$ sample. These changes are attributed to a typical transition from Ce^{4+} to Ce^{3+}, and such changes have been observed in $CeO_{2-\delta}$.[20,37] The O K-edges of samples with $R_{sm} = 0.33$ and 0.67 also exhibited different shapes, as shown in Fig. 7(c) and 7(d), respectively. For the sample with $R_{sm} = 0.33$, the edge had sharp characteristic peaks at 529.3, 532.0, and 536.2 eV, respectively. In contrast, for the sample with $R_{sm} = 0.67$, the O K-edge had rather broad peaks at 533.7 and 536.2 eV; this peak broadening is probably attributable to the lowest 4f orbital of cerium being filled, leaving no unoccupied part of the orbital that could be *p*-like and thus contribute to the O K-edge.

For the trivalent cerium ion, Ce^{3+}, a localized 4f moment is expected to be responsible for the ion's relatively larger magnetization in a magnetic field than that of Ce^{4+}, since Ce^{3+} has a ground state consisting of six-fold degenerate 4f states, $^2F_{5/2}$, and a total angular momentum of $J = 5/2$ while Ce^{+4} has $J = 0$. The temperature dependence of the magnetic susceptibility, $\chi(T)$, obeys Curie's law ($\chi \approx C/T$) below $T = 30$ K, as shown in Fig. 8, but deviates from the lower-temperature Curie law at higher temperatures, owing to thermal excitations of the excited crystal-field states. This characteristic temperature dependence of $\chi(T)$ results from a crystal-field effect. Since the Ce ion is located in the cubic-crystal field at the centre position of the face-centered cubic (FCC) unit cell, with oxygen atoms at the corners in the fluorite (CaF_2) structure, the six-fold degenerate 4f states of Ce^{3+} split into four-fold degenerate Γ_8 states and doubly degenerate Γ_7 states. On the other hand, in case of the crystal structure C-Ce_2O_3,[24] which is expected to be formed at $R_{sm} \sim 80\%$, all cerium ions are trivalent and located in the centers of O_6-octahedra. In this case, as is expected, the Γ_7 state is the ground state while for the Ce^{3+} ion located at the body center of FCC unit cell the Γ_8 state is the ground state. A possible explanation for this is that the coordination number of Ce ion is reduced with increasing R_{sm}, which is consistent with density functional theory (DFT) calculations[38] that show that the Ce^{3+} ion locates along with the oxygen vacancy. Therefore we can assume the octahedral-cubic crystal field, that is, the Γ_7 doublet is the ground state and the Γ_8 quartet locates at Δ in energy above the Γ_7 level. In fact, as shown in Fig. 8, the susceptibility-temperature data can be fitted well with this assumption. Figure 9(a) shows the concentration of Ce^{3+} ions, $n(Ce^{3+})$, and Δ as a function of R_{sm}. Notably, the gradient of $n(Ce^{3+})$ with respect to R_{sm} changes steeply, with the corresponding changes in XANES spectra occurring as shown in Fig. 9(b). It is recently indicated, similar to our findings, that oxygen vacancy of $CeO_{2-\delta}$ nanoparticles with $D = 2.7$–3.5 nm

produced by thermal decomposition method is stabilized with surfactant.[39] Surprisingly, the vacancy in $CeO_{2-\delta}$ nanocrystal seems to bring about a small ferromagnetic moment (0.01–0.12 emu/g) at room temperature. In contrast, it should be emphasized that this room-temperature ferromagnetism is hardly detectable in the surface-modified nanoparticle samples examined in this study.

Assuming that the valence change of cerium is predominantly attributable to the formation of oxygen vacancies in $CeO_{2-\delta}$ nanocrystals,[38–41] the previous analysis suggests that these vacancies are created and/or stabilized by the bonding of the oleic acid molecules to the surface. Around $R_{sm} \sim 80\%$ the cerium ion is trivalent. Therefore, the valence of cerium is related to the number of ligand molecules bound on the surface of the nanoparticle. In fact, as shown in Fig. 9(c), the ratio of the number of oxygen vacancies to the number of ligand molecules (per crystal), N_{ov}/N_{sm} is approximately 0.18. Although it is not obvious whether the ratio is a constant of R_{sm}, this suggests one oxygen vacancy is stabilized by approximately 5–6 oleic acid molecules adsorbed on the nanocrystal surface.

IV. DISCUSSION AND CONCLUSION

The detailed analysis presented in this paper has demonstrated that nonmodified ceria nanocrystals showed no substantial valence change under ambient conditions with particle sizes greater than $D \sim 3$ nm, whereas nanocrystals with surfaces modified with oleic acid exhibited a strong size and surface modification-dependent variation in valence states below diameters of 7 nm [Fig. 6(c) and (d)]. These experimental results indicate that the modification of the surface with oleic acid ligands can induce a valence transition from Ce^{+4} to Ce^{+3} in the nanocrystals. This provides important insights for understanding the electronic and structural changes that result from interactions between surface ligands and the electronic states of metal oxide nanocrystals.

These findings imply that the static valence transformation from Ce^{4+} to Ce^{3+} is dependent strongly on both the crystal size and the surface coverage of organic ligands. One possible explanation for this is that neutral oxygen vacancies (the formation of which results in the Ce ion valence change) are stabilized by ligand molecules binding to the nanoparticle surface. An alternative explanation is that the valence change is caused by changes in the coordination of surface ions, which is dependent on the crystal shape and structure of the surface (which may be modified by the molecular adsorbates).

As discussed previously, there is a large discrepancy in $a(D)$ among previous studies[18,20,22,41] as well as between those studies and our present study [Fig. 2(b)]. This discrepancy indicates that, as the crystal size decreases, $\Delta a/a$ is a function not only of valence state but also of the surface structure of the nanocrystals, namely, the surface morphology (exposed crystallographic surfaces) and the extent of surface modification by organic molecules. This may be attributable to different changes in the crystal structure caused by the formation of oxygen vacancies on different crystallographic surfaces. If the formation of vacancies on either the (111) or (001) facets resulted in a greater or smaller change in average interatomic distances, the lattice parameter would depend on the morphology, which is suggested by DFT simulations.[40,42] In addition, changes in surface structure may occur because of the interaction with adsorbed molecules, which would result in the lattice parameter being dependent on both the coverage and morphology. DFT studies have demonstrated that the average interatomic distances in small, unmodified ceria nanoparticles are most significantly affected by the creation of oxygen vacancies,[42] however, this was only considering octohedral particles with (111) exposed surfaces.

Using XRD and high-resolution TEM, F. Zhang *et al.*[22] observed the exposed (111) surface in most of their ceria nanoparticles, whereas Wu *et al.*[20] observed their ceria nanoparticles to be spherical. Tsunekawa *et al.*[18,19] have indicated that their ceria nanoparticles are a mixture of octahedral and spherical particles surrounded by a (111) plane and different crystallographic surfaces, respectively.[41,43]

Atomistic simulations have demonstrated that the morphology of unmodified ceria nanoparticles are truncated octohedra[44] consisting of both (111) and (001) terminating surfaces, with the (111) surface dominating because of its lower surface energy.[45] The energy required to form oxygen-atom vacancies on both of these surfaces is relatively high: for the (111) surface the vacancy-formation energy is calculated (with DFT and with respect to half an O_2 molecule) as 3.3 eV[40] and on the (001) surface as 2.9 eV.[40] However, recent calculations have demonstrated that the oxygen vacancy formation at low-coordinated oxygen sites at corners and edges of truncated octohedral nanoparticles requires much lower energies (as low as 0.58 eV).[46] The proportion of low-coordinated oxygen atoms increases as the nanoparticle size decreases, and therefore the valence transformation is greatly facilitated. DFT calculations of the formation of oxygen vacancies at both (111) and (001) facets have demonstrated that the extraction of a neutral oxygen from the surface (and subsurface) results in the reduction of two neighboring Ce(IV) atoms to Ce(III), creating a new state in the ceria band gap below the unoccupied Ce 4f states, which is consistent with these results.[40,47]

DFT calculations have also demonstrated how carboxylic acids can stabilize oxygen vacancies on ceria surfaces. In Gordon *et al.*[48] the adsorption energy of formic acid on the (111) surface of ceria is calculated to be 1.07 eV and the acid is deprotonated on the surface (the molecule binds as a carboxylate, as suggested by the IR spectroscopy in this study). The binding energy of the molecule to a single oxygen vacancy, however, increases to 3.95 eV, which is larger than the vacancy formation energies on both the (111) and (001) surfaces. These calculations suggest that carboxylic acid molecules can facilitate the formation of oxygen vacancies at ceria surfaces [particularly at the low-coordinated sites and on the (001) surface], which can explain the overall valence change observed in this study as the coverage of the molecules is increased. However, further calculations are required to fully understand how carboxylic groups interact with low-coordinated vacancies and vacancies in the (001) surface, which is key to the valence transformation and its relationship to the coverage of the molecules. Another key component to understanding the ratio between the number

of surface ligands and the number of oxygen vacancies is the interaction between the oleic acid molecules, which will contribute to surface energies and affect both the relative coverage on different surfaces and the morphology of the particles.

After removing surface bonding molecules (hexanoic acid) by treating the samples in air at 150 °C, the morphology of ceria nanocrystals does not change and the crystal structure is stable.[49] Consequently, the crystals possess a high proportion of highly activated crystallographic surfaces, such as (001) planes, realized by using the *in-situ* surface modification. These particles then reversibly show an unexpectedly high oxygen storage capacity performance even at extremely low temperatures.[49]

ACKNOWLEDGMENTS

We would like to express our appreciation to Dr. S. Tsunekawa in IMR, and Drs. H. Isago and H. Suzuki in NIMS for valuable discussions. This work was partially supported by the Grant-in-Aid for Scientific Research, KAKENHI, (17206078, 19310063, and 20226015).

*naka.takashi@nims.go.jp

[1] E. Takayama-Muromachi, Y. Uchida, M. Ishii, T. Tanaka, and K. Kato, Jpn. J. Appl. Phys. Part 2 **26**, L1156 (1987).
[2] F. Iga and Y. Nishihara, J. Phys. Soc. Jpn. **61**, 1867 (1992).
[3] È. L. Nagaev, in *Colossal Magnetoresistance and Phase Separation in Magnetic Semiconductors* (Imperial College Press, London, 2002), Ch. 7, p. 297.
[4] A. Trovarelli, Catal. Rev. Sci. Eng. **38**, 439 (1996).
[5] A. J. Zarur and J. Y. Ying, Nature **403**, 65 (2000).
[6] S. D. Park, J. M. Vohs, and R. J. Gorte, Nature **404**, 265 (2000).
[7] T. Hyeon, S. S. Lee, J. Park, Y. Chung, and H. B. Na, J. Am. Chem. Soc. **123**, 2798 (2001).
[8] J. Rockenberger, E. C. Scher, and A. P. Alivisatos, J. Am. Chem. Soc. **121**, 11595 (1999).
[9] J. Park, K. An, Y. Hwang, J. G. Park, H. J. Noh, J. Y. Kim, J. H. Park, N. M. Hwang, and T. Hyeon, Nat. Mater. **3**, 891 (2004).
[10] X. Wang, J. Zhuang, Q. Peng, and Y. D. Li, Nature **437**, 121 (2005).
[11] H. Weingartner and E. U. Franck, Angew. Chem. Int. Ed. **44**, 2672 (2005).
[12] T. Adschiri, Y. Hakuta, and K. Arai, Ind. Eng. Chem. Res. **39**, 4901 (2000).
[13] K. J. Ziegler, R. C. Doty, K. P. Johnston, and B. A. Korgel, J. Am. Chem. Soc. **123**, 7797 (2001).
[14] P. S. Shah, T. Hanrath, K. P. Johnston, and B. A. Korgel, J. Phys. Chem. B **108**, 9574 (2004).
[15] J. Zhang, S. Ohara, M. Umetsu, T. Naka, Y. Hatakeyama, and T. Adschiri, Adv. Mater. **19**, 203 (2007).
[16] M. Taguchi, S. Takami, T. Naka, and T. Adschiri, Crystal Growth & Design, **9**, 5297 (2009).
[17] T. Arita, Y. Ueda, K. Minami, T. Naka, and T. Adschiri, Ind. Eng. Chem. Res. **49**, 1947 (2010).
[18] S. Tsunekawa, T. Fukuda, and A. Kasuya, J. Appl. Phys. **87**, 1318 (2000).
[19] S. Tsunekawa, K. Ishikawa, Z. Q. Li, Y. Kawazoe, and A. Kasuya, Phys. Rev. Lett. **85**, 3440 (2000).
[20] L. J. Wu, H. J. Wiesmann, A. R. Moodenbaugh, R. F. Klie, Y. M. Zhu, D. O. Welch, and M. Suenaga, Phys. Rev. B **69**, 125415 (2004).
[21] S. Deshpande, S. Patil, S. V. N. T. Kuchibhatla, and S. Seal, Appl. Phys. Lett. **87**, 133113 (2005).
[22] F. Zhang, S.-W. Chan, J. E. Spanier, E. Apak, Q. Jin, R. D. Robinson, and I. P. Herman, Appl. Phys. Lett. **80**, 127 (2002).
[23] K. Kaneko, K. Inoke, B. Freitag, A. B. Hungria, P. A. Midgley, T. W. Hansen, J. Zhang, S. Ohara, and T. Adschiri, Nano. Lett. **7**, 421 (2007).
[24] E. A. Kummerle and G. Heger, Journal of Solid State Chemistry **147**, 485 (1999).
[25] V. Bolis, G. Magnacca, G. Cerrato, and C. Morterra, Therm. Acta. **379**, 147 (2001).
[26] C. Binet and M. Daturi, Catal. Today. **70**, 155 (2001).
[27] Y. G. Aronoff, B. Chen, G. Lu, C. Seto, J. Schwartz, and S. L. Bernasek, J. Am. Chem. Soc. **119**, 259 (1997).
[28] J. E. Tackett, Appl. Spectrosc. **43**, 483 (1989).
[29] Y. Sahoo, H. Pizem, T. Fried, D. Golodnitsky, L. Burstein, C. N. Sukenik, and G. Markovich, Langmuir **17**, 7907 (2001).
[30] L. F. Shen, P. E. Laibinis, and T. A. Hatton, Langmuir **15**, 447 (1999).
[31] G. Kaindl, G. Schmiester, and E. V. Sampathkurmaran, Phys. Rev. BI **38**, 10174 (1988).
[32] A. V. Soldatov, T. S. Ivanchenko, S. D. Longa, A. Kotani, Y. Iwamoto, and A. Bianconi, Phys. Rev. B **50**, 5074 (1994).
[33] L. Douillard, M. Gautier, N. Thromat, and J. P. Duraud, Nucl. Instr. Meth. Phys. Res. B **97**, 133 (1995).
[34] T. W. Capehart, R. K. Mishra, and J. F. Herbst, J. Appl. Phys. **72**, 676 (1992).
[35] P. Nachimuthu, W. Shih, R. Liu, L. Jang, and J. Chen, J. Solid State Chem. **149**, 408 (2000).
[36] D. Bazin, D. Sayers, J. J. Rehr, and C. Mottet, J. Phys. Chem B **101**, 5332 (1997).
[37] L. A. J. Garvie and P. R. Buseck, J. Phys. Chem. Sol. **60**, 1943 (1999).
[38] N. V. Skorodumova, S. I. Simak, B. I. Lundqvist, I. A. Abrikosov, and B. Johansson, Phys. Rev. Lett. **89**, 166601 (2002).
[39] S.-Y. Chen, Y.-H. Lu, T.-W. Huang, D.-C. Yan, and C.-L. Dong, J. Phys. Chem. C **114**, 19576 (2010).
[40] M. Nolan, S. C. Parker, and G. W. Watson, Surf. Sci. **595**, 223 (2005).
[41] S. Tsunekawa, S. Ito, and Y. Kawazoe, Appl. Phys. Lett. **85**, 3845 (2004).
[42] C. Loschen, A. Migani, S.T. Bromley, F. Illas, and K. M. Neyman, Phys. Chem. Chem. Phys. **10**, 5730 (2008).
[43] S. Tsunekawa, R. Sivamohan, S. Ito, A. Kasuya, and T. Fukuda, Nanostructured Materials **11**, 141 (1999).
[44] T. Sayle, S. C. Parker, and D. C. Sayle, Chem. Commum. **21**, 2438 (2004).

[45] M. Nolan, S. Grigoleit, D. C. Sayle, S. C. Parker, and G. W. Watson, Surf. Sci. **576**, 217 (2004).

[46] A. Migani, G. N. Vayssilov, S. T. Bromley, F. Illas, and K. M. Neyman, J. Materials Chem. **20**, 10535 (2010).

[47] M. V. Ganduglia-Pirovano, J. L. F. Da Silva, and J. Sauer, Phys. Rev. Lett. **102**, 026101 (2009).

[48] W. O. Gordon, Y. Xu, D. R. Mullins, and S. H. Overbury, Phys. Chem. Chem. Phys. **11**, 11171 (2009).

[49] J. Zhang, H. Kumagai, K. Yamamura, S. Ohara, S. Takami, A. Morikawa, H. Shinjoh, K. Kaneko, T. Adschiri, and A. Suda, Nano. Lett. **11**, 361 (2011).